Supplementary Information

Stretchable liquid metal transmission lines as distributed probes of multimodal deformations

Andreas Leber, Chaoqun Dong, Rajasundar Chandran, Tapajyoti Das Gupta, Nicola Bartolomei & Fabien Sorin

This file includes Supplementary Notes 1-6 and Supplementary Figures 1-13.

Supplementary Note 1: Calculation of the characteristic impedance based on the time-domain reflectometry waveform

The characteristic impedance of a transmission line can be deduced directly from a time-domain reflectometry measurement. The decisive feature of the waveform is the voltage amplitude across the transmission line at a time where the input signal has risen to its full level, but no reflected waves have reached the interrogated end. The characteristic impedance Z_0 is calculated based on the measured voltage U as well as the generator's input voltage U_g and internal resistance R_g[1]:

$$Z_0 = R_g \cdot \frac{1}{\left(\frac{U_g}{U} - 1\right)}$$

When plugging in the values obtained for the measurement of a standard coaxial cable (Supplementary Fig. 1), we do indeed find the expected characteristic impedance of 50 Ω. Transmission lines with custom connectors are more difficult to evaluate, because the contact resistance of the line connector offsets the voltage level.

Supplementary Note 2: Effect of medium surrounding the soft transmission lines on time-domain reflectometry measurement

The shield quality of different transmission line designs was evaluated by introducing a section of the line in a medium of higher dielectric constant than air (Fig. 2c, d). For designs where the electrical field is not contained within the structure, the medium affects the propagation of signals through the line, because it changes the apparent dielectric constant. In the case of time-domain reflectometry, the effect on the measured waveform is twofold: (i) a reflection at the air-medium interfaces with an amplitude that depends on the change in apparent dielectric constant, and (ii) a time shift of the reflection at the open-circuit termination. The effect is particularly noticeable for the two-wire design because it does not have an effective shield. As the employed media in the test are water and ethanol with higher dielectric constants than air, the reflection at the interface is negative. Additionally, the propagation speed in the section with the higher apparent dielectric constant is reduced, resulting in a positive time shift of the reflection at the open-circuit termination. Thus, time-domain reflectometry reveals both the nature of the medium, identified by its dielectric constant, and the section of the transmission line which is surrounded by it[2].

Supplementary Note 3: Theoretical considerations of loss in soft transmission lines

The liquid metal transmission lines are approximated as low-loss lines, for which the attenuation coefficient α can be expressed by[3]:

$$\alpha \simeq \frac{1}{2} \cdot \left(\frac{R}{Z_0} + G \cdot Z_0\right)$$

where Z_0 is the characteristic impedance and R and G the series resistance and shunt conductance per length, respectively. In our analysis, we focus on the resistive term, which is expected to dominate over the dielectric term, because the loss tangent of the dielectric SEBS is low (0.07 at 3.5 GHz)[4] while the resistivity of the conductor Ga-In-Sn is high ($3 \cdot 10^{-7}$ Ωm)[5]. The resistance per length due to skin effect is[6]:

$$R = \frac{R_S}{A}$$

where R_S is the skin resistance and A the conductor surface area per length. The skin resistance is[6]:

$$R_S = \sqrt{\frac{\omega\mu}{2\sigma}}$$

where ω is the angular frequency, μ the permeability, and σ the conductivity. Thus, the resistive term of the attenuation coefficient is

$$\alpha_c \simeq \frac{1}{2} \cdot \frac{1}{Z_0 \cdot A} \cdot \sqrt{\frac{\omega\mu}{2\sigma}}$$

This expression gives an insight into the relevant parameters, which dictate the loss in the transmission lines, and can be used to explain results that were obtained experimentally (Fig. 2f), including the square root relationship between frequency and the attenuation coefficient, the lower loss of Cu lines compared to Ga-In-Sn lines due to a higher conductivity, the decrease in attenuation coefficient for increased surface area (only for frequencies below 1 MHz due to the proximity effect which is not considered in the equation), and finally the controlled reduction in loss through an increase in characteristic impedance.

For a low-loss transmission line, the characteristic impedance is[3]:

$$Z_0 \simeq \sqrt{\frac{L}{C}}$$

where L is the series inductance and C the shunt capacitance per length. Thus, it depends on the geometry of the transmission line. For a coaxial structure, it is[7]:

$$Z_0 \simeq \frac{1}{2\,\pi} \sqrt{\frac{\mu}{\varepsilon}} \ln\left(\frac{D}{d}\right)$$

where μ is the permeability, ε the permittivity, and D and d the outer and inner conductor diameter respectively. For the triangular structure, the characteristic impedance is[8]:

$$Z_0 \simeq \frac{1}{6\pi} \cdot \sqrt{\frac{\mu}{\varepsilon}} \cdot \ln\left(H + \sqrt{H^2 - 1}\right)$$

where H is the geometric factor depending on the center-to-center spacing between center to shield wire s and the center and shield wire radius r_i and r_o, respectively:

$$H = \frac{(s^2 - {r_o}^2)^3 - {r_i}^6}{{r_i}^3[(s + r_o)^3 - (s - r_o)^3]}$$

We calculate the characteristic impedances of transmission line geometries considered in the analysis of loss and compare them to values obtained by time-domain reflectometry in Supplementary Table 1. The geometries are detailed in Supplementary Fig. 5. While, the theoretical and experimental values correspond in trend, a discrepancy does exist, which is attributed to a measurement error caused by the contact resistance of the line connectors. Nonetheless, the controlled increase of the characteristic impedance is reflected by a decrease in loss, as shown in Fig. 2f.

Supplementary Table 1: Characteristic impedances of transmission lines obtained theoretically and experimentally.

Transmission line design	Theoretical value (Ω)	Experimental value (Ω)
Triangular with low spacing-to-diameter ratio	48	61
Triangular with medium spacing-to-diameter ratio	79	77
Triangular with large spacing-to-diameter ratio	95	120
Coaxial	44	66

Supplementary Note 4: Calculation of magnitude of resistive and capacitive discontinuities in soft transmission lines

Time-domain reflectometry measurements convey many pieces of information on discontinuities along the transmission lines, including nature and magnitude. A single resistive discontinuity in series is known to cause a step in the waveform. The reflection event is quantified by the reflection coefficient, which is the ratio of reflected to incident voltage. The magnitude of the resistance R_S can be deduced from the reflection coefficient ρ[1]:

$$R_S = 2 \cdot Z_0 \cdot \left(\frac{\rho}{1-\rho}\right)$$

where Z_0 is the characteristic impedance of the line. A shunt capacitive discontinuity, however, causes a negative peak in the waveform. Its magnitude C_P can be approximated by the peak value V_{peak}[9]:

$$C_P \simeq \frac{|V_{peak}|}{1.1 \cdot Z_0} \cdot \frac{t_{rise}}{U_i}$$

where t_{rise} is the rise time and U_i the amplitude of the incident step. Thus, both types of discontinuities can be quantified using the reflected voltage.

Supplementary Note 5: Calculation of distributed resistance of soft transmission lines

In Supplementary Note 4, it was discussed how the magnitude of a resistive discontinuity can be calculated using voltage levels obtained from the time-domain reflectometry waveforms. This is an straightforward process when only a single discontinuity is present on the line. However, in the case of multiple discontinuities, multiple transmissions and reflections occur. For instance in the case of two discontinuities, the reflection at the second discontinuity is diminished by the transmission-reflection at the first discontinuity before reaching the monitored line end[1].

A recursive algorithm is employed to calculate the true reflection coefficient ρ_i for each time step i in the waveform[10]:

$$\rho_i = \frac{\Delta U_i}{U_0 \cdot \prod_{j=0}^{i-1}(1+\rho_j)}$$

where ΔU_i is the amplitude of a discontinuity-generated measured voltage step and U_0 the incident voltage. In this strategy, only the first reflections at the discontinuities are considered, which are partly transmitted at previous discontinuities. The geometric series of internal multiple reflections, each weaker than the last, is neglected. Based on the calculated true reflection coefficient, the resistance is calculated using the equation in Supplementary Note 4, resulting in a resistance distribution for the soft transmission lines (Fig. 3f).

Supplementary Note 6: Theoretical considerations of distance dependency of spatial resolution for pressure localization on soft transmission line probes

It was found that the spatial resolution of the pressure localization on the soft transmission lines is limited by the length-dependent pulse broadening (Fig. 3g). This phenomenon is attributed to the frequency-dependent skin effect, which is the dominant mechanism for attenuation at microwave frequencies. When considering a perfect unit step function as an input waveform, the changed shape of step response can be described by[6]:

$$U(t) = U_0 \cdot erf\left(\frac{z\,k}{2\sqrt{t}}\right) = U_0 \cdot erf\left(\sqrt{\frac{\tau}{t}}\right)$$

where U_0 is the amplitude as the input step, erf the error function, z the distance down the line, k a constant for the skin effect, and t the time. The time constant τ can be employed to quantify the pulse broadening and is proportional to the square of the line distance. Indeed, a square relationship between the spatial resolution and the line distance was found experimentally (Fig. 3h).

References:

1. Strickland, J. A., Zimmerman, H. A., Long, G. & Frye, G. *Time-domain Reflectometry Measurements*. (Tektronix, 1970).
2. Cataldo, A., De Benedetto, E. & Cannazza, G. *Broadband Reflectometry for Enhanced Diagnostics and Monitoring Applications*. **93**, (Springer Berlin Heidelberg, 2011).
3. Pozar, D. M. *Microwave Engineering*. (John Wiley & Sons, Inc., 2012).
4. Zandvakili, M., Honari, M. M., Mousavi, P. & Sameoto, D. Gecko-Gaskets for Multilayer, Complex, and Stretchable Liquid Metal Microwave Circuits and Antennas. *Adv. Mater. Technol.* **2**, 1700144 (2017).
5. Rogers, J. A., Ghaffari, R. & Kim, D.-H. *Stretchable Bioelectronics for Medical Devices and Systems*. (Springer International Publishing, 2016). doi:10.1007/978-3-319-28694-5
6. Collier, R. J. *Transmission lines : equivalent circuits, electromagnetic theory, and photons*. (Cambridge University Press, 2013).
7. Wadell, B. C. *Transmission line design handbook*. (Artech House, 1991).
8. Ball, J. A. R. Characteristic impedance of unbalanced TDR probes. *IEEE Trans. Instrum. Meas.* **51**, 532–536 (2002).
9. Lee, T. H. *Planar Microwave Engineering*. (Cambridge University Press, 2004). doi:10.1017/CBO9780511812941
10. Hsue, C. W. & Pan, T. W. Reconstruction of nonuniform transmission lines from time-domain reflectometry. *IEEE Trans. Microw. Theory Tech.* **45**, 32–38 (1997).

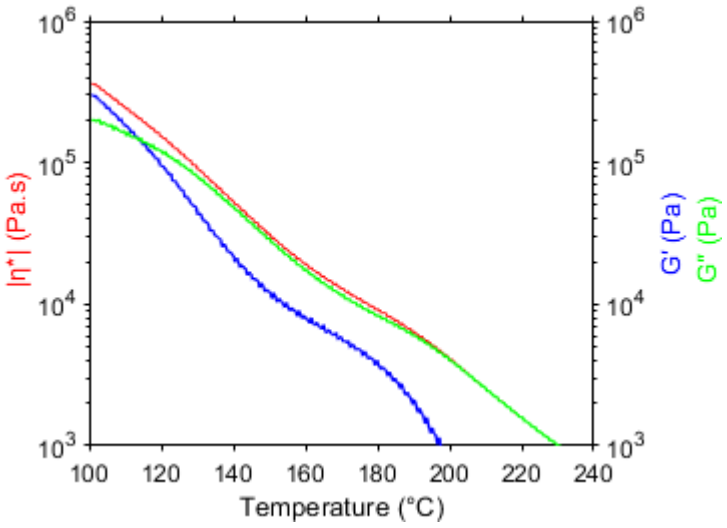

Supplementary Fig. 1| Rheological properties of SEBS illustrated by the magnitude of the complex viscosity |η*|, storage modulus G', and loss modulus G'' as a function of temperature. The temperature-dependent material flow is characterized by a loss modulus that decreases steadily with temperature and crosses over the rapidly decreasing storage modulus.

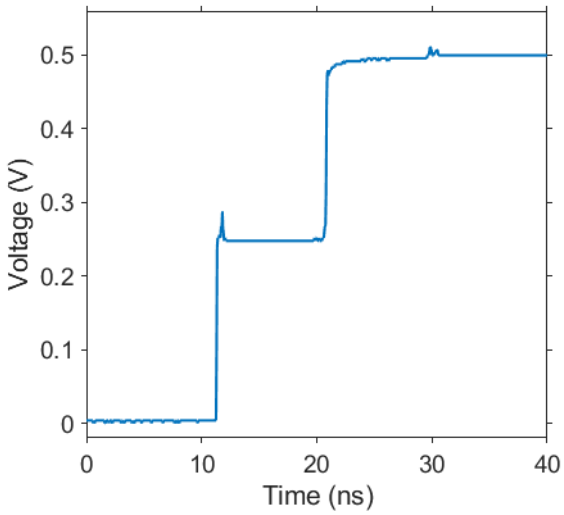

Supplementary Fig. 2| Time-domain reflectometry waveform for standard coaxial cable with characteristic impedance 50 Ω, showing the input pulse and reflection at open-circuit termination.

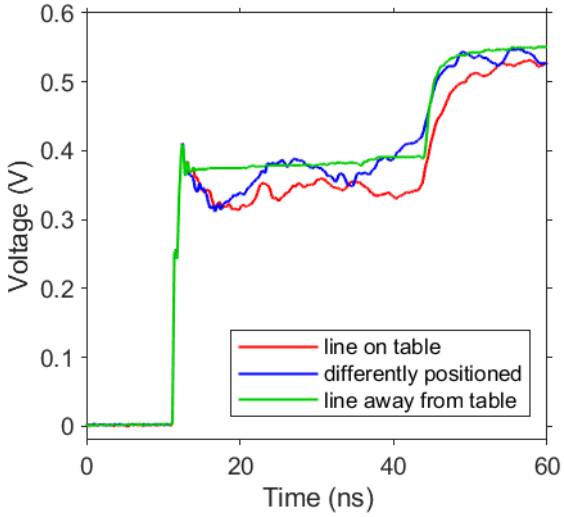

Supplementary Fig. 3| Time-domain reflectometry waveforms for a liquid metal transmission line with the two-wire design, which is placed on a metallic table in two different configurations and suspended in air at a large distance to the table, illustrating the undesired interactions of the line with its environment.

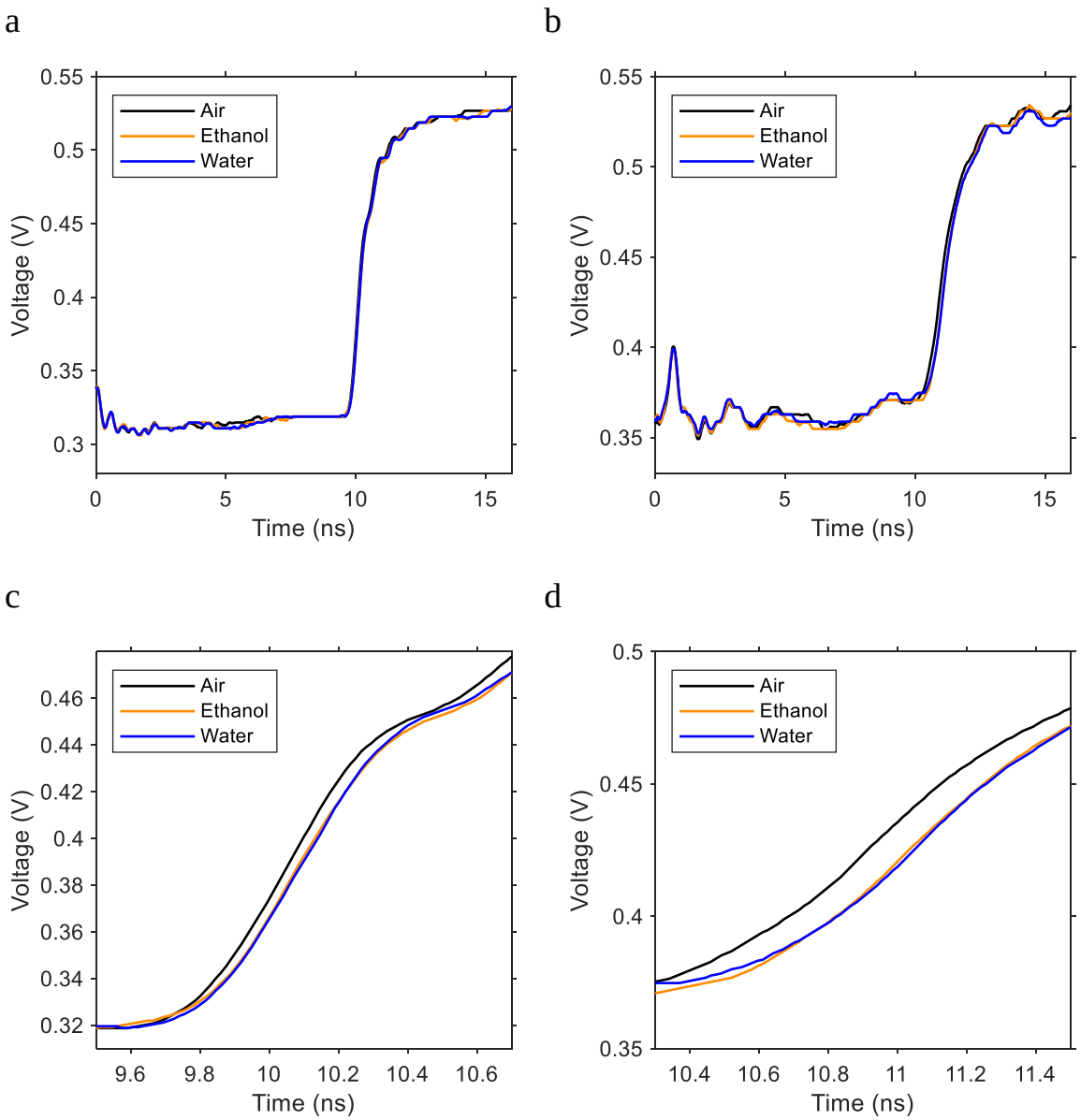

Supplementary Fig. 4| Time-domain reflectometry waveforms for triangular (a) and stripline (b) transmission lines before and after a section of the line is submersed in water and ethanol. The initial signal rise and connector ringing are cut for clarity. Enlarged plots of the reflection at the open-circuit termination for triangular (c) and stripline (d) transmission lines are shown, underlining the time delay induced by the medium.

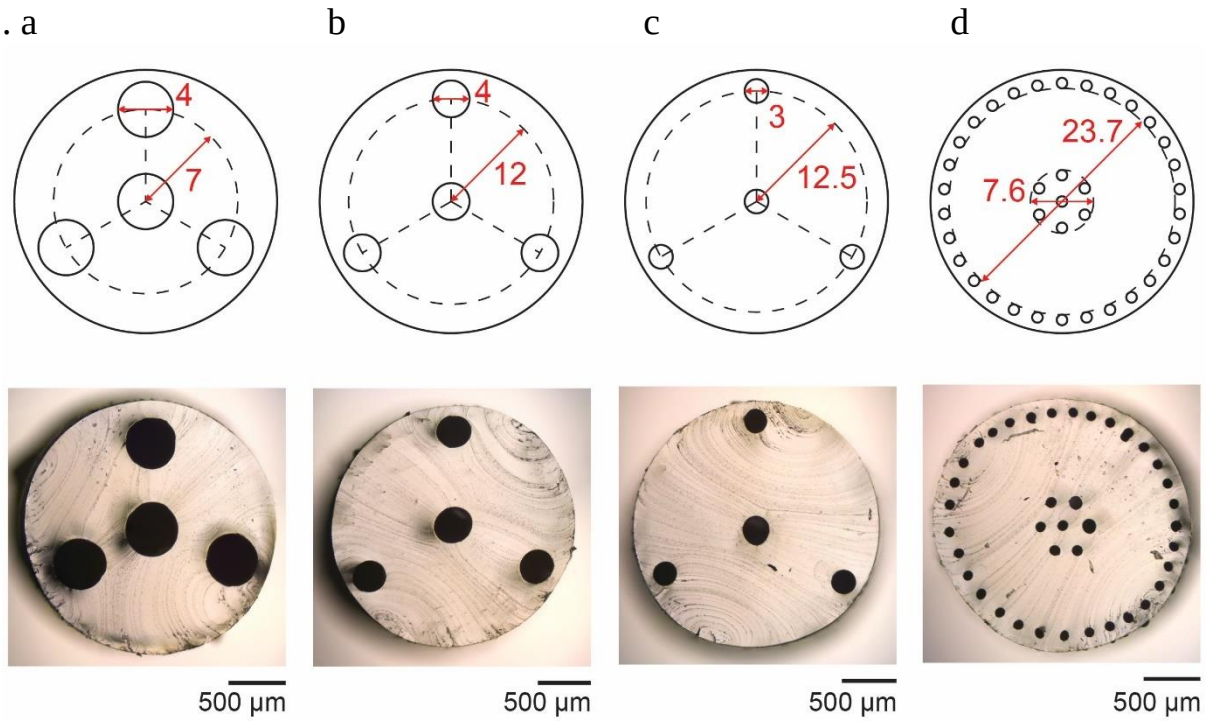

Supplementary Fig. 5| Geometries of considered designs for liquid metal transmission lines, illustrated by schematics with preform dimensions in mm (top) and micrographs (bottom). a, b, and c, Triangular structures with increasing conductor spacing-to-diameter-ratios, and d, coaxial structure.

a b

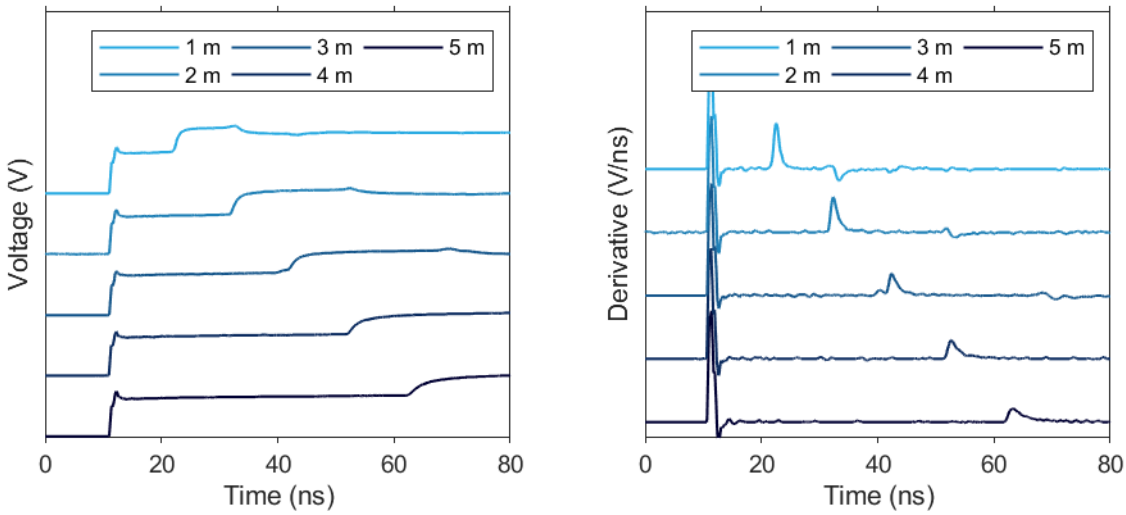

Supplementary Fig. 6| Time-domain reflectometry waveforms observed for liquid metal triangular transmission lines of increasing lengths (a) and derivatives of waveforms (b), illustrating the increase in broadness of reflections at the open circuit termination.

. a b

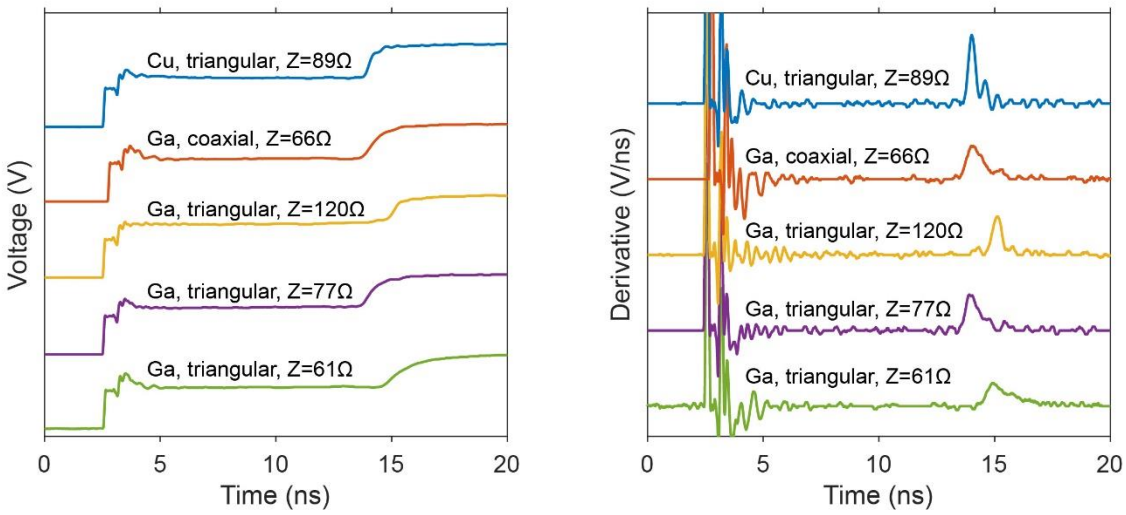

Supplementary Fig. 7| Time-domain reflectometry waveforms (a) and waveform derivatives (b) of transmission lines with different conductor materials (liquid metal Ga, solid copper Cu), structure type (triangular, coaxial), and characteristic impedance (Z), illustrating the correlation between determined attenuation coefficient (Fig. 2f) and broadening of the reflection at the open-circuit termination.

. a

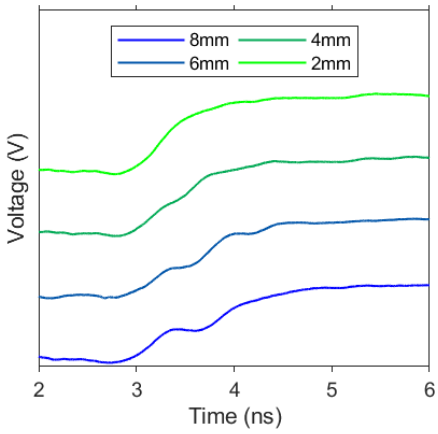
8mm
4mm
6mm
2mm
Voltage (V)
2
3
4
5
6
Time (ns)

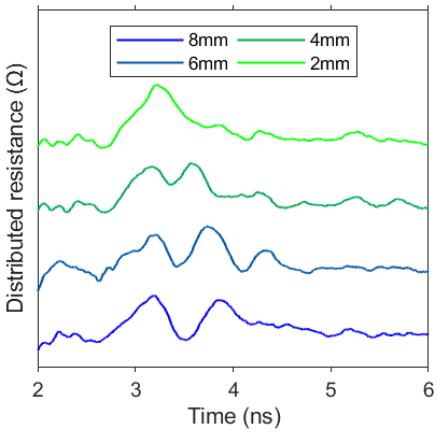
8mm
4mm
6mm
2mm
Distributed resistance (Ω)
2
3
4
5
6
Time (ns)

. b

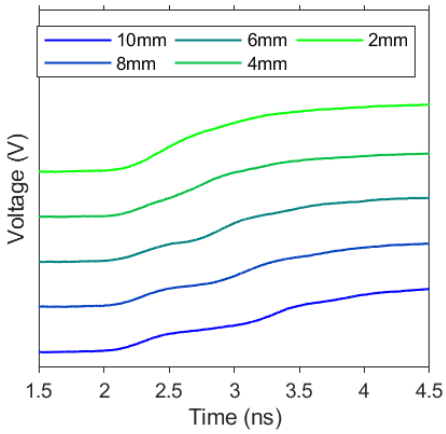
10mm
6mm
2mm
8mm
4mm
Voltage (V)
1.5
2
2.5
3
3.5
4
4.5
Time (ns)

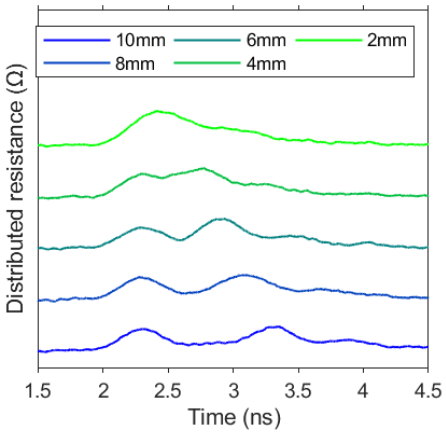
10mm
6mm
2mm
8mm
4mm
Distributed resistance (Ω)
1.5
2
2.5
3
3.5
4
4.5
Time (ns)

. c

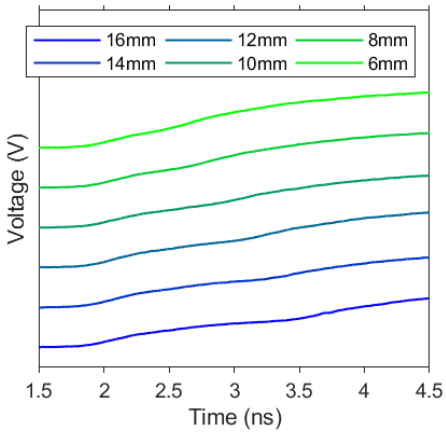
16mm
12mm
8mm
14mm
10mm
6mm
Voltage (V)
1.5
2
2.5
3
3.5
4
4.5
Time (ns)

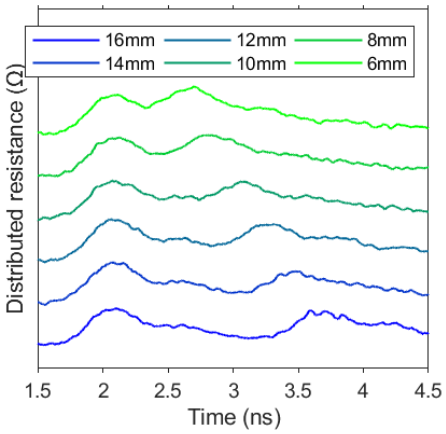
16mm
12mm
8mm
14mm
10mm
6mm
Distributed resistance (Ω)
1.5
2
2.5
3
3.5
4
4.5
Time (ns)

d

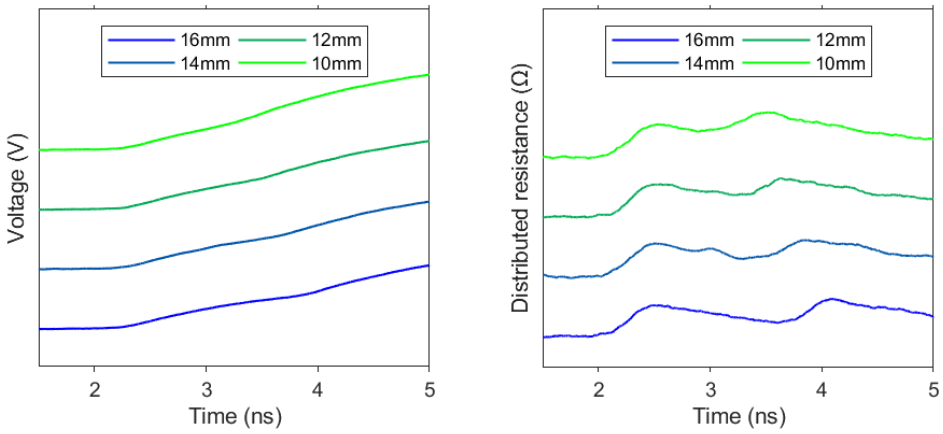

. e

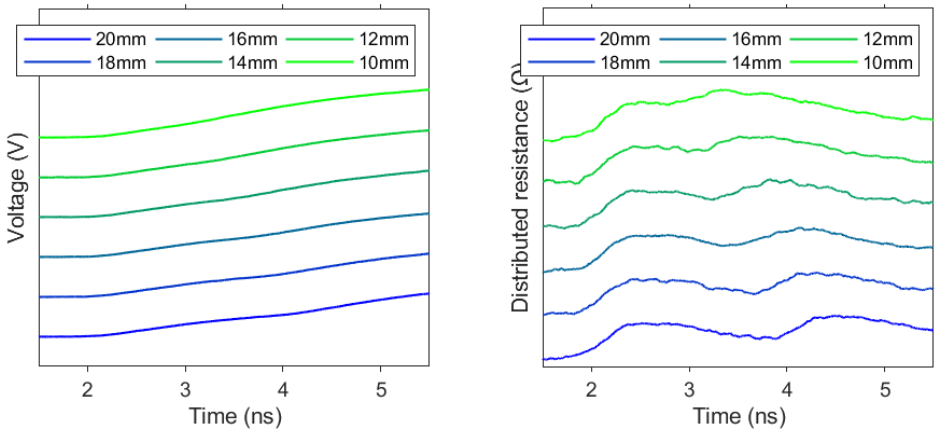

.
f

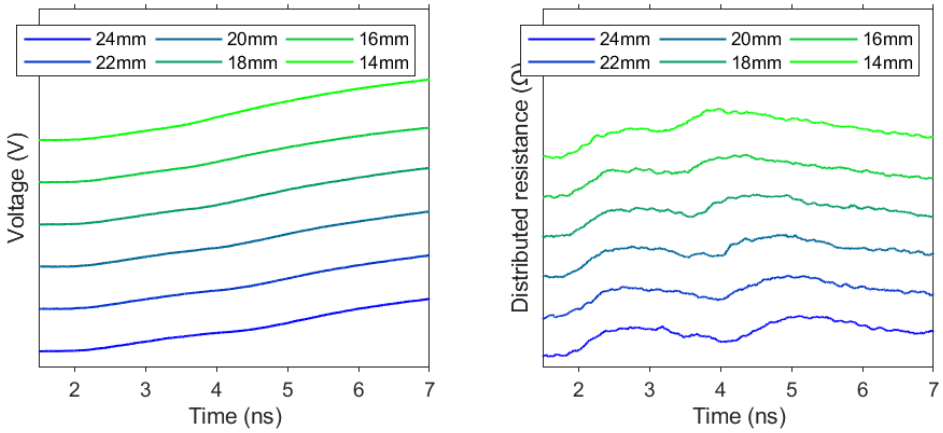

Supplementary Fig. 8| Time-domain reflectometry waveforms (left) and calculated distributed resistance (right) of two pressure points being applied with different spacings between them, as indicated in the legends, for the positions along the length of the transmission lines of a, 0.2m, b, 1m, c, 2m, d, 3m, e, 4m, and f, 5m. The spatial resolution of the pressure localization is determined using this data and is shown in Fig. 3h.

a b c

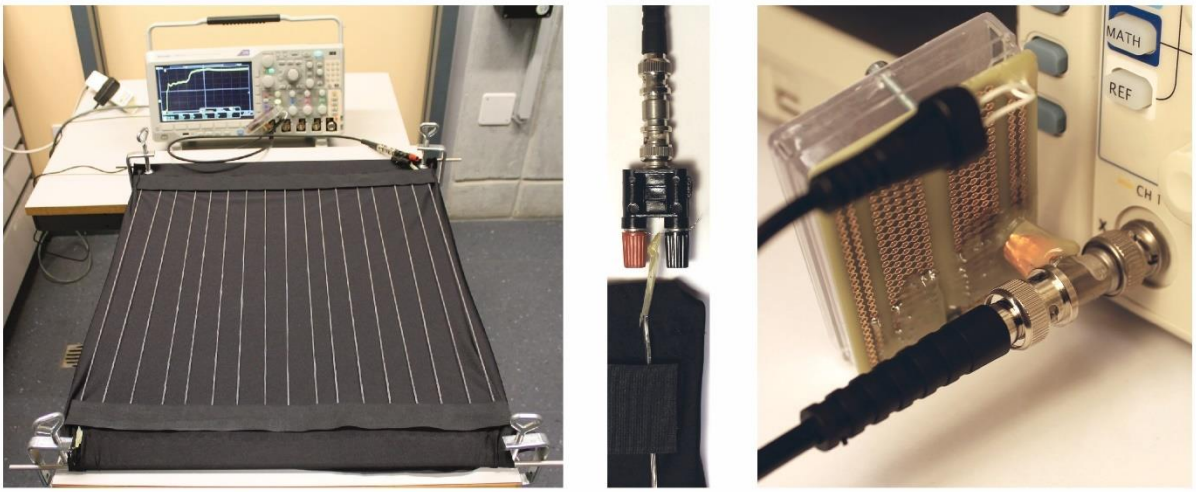

Supplementary Fig. 9| a, The electronic textile protype consists of a triangular liquid metal transmission line of length 10 m that is integrated on a stretchable fabric (50 cm x 50 cm) and fixed in place by Velcro bands. b, The line is interfaced through a single point, where the outer and center conductors of the line are connected to the negative and positive pole, respectively, of a standard BNC-to-wire adapter. c) A standard 50 Ω coaxial cable is used to connect the electronic textile to a T adapter, of which the other two leads are connected to the pulse generator and oscilloscope, respectively.

a

b

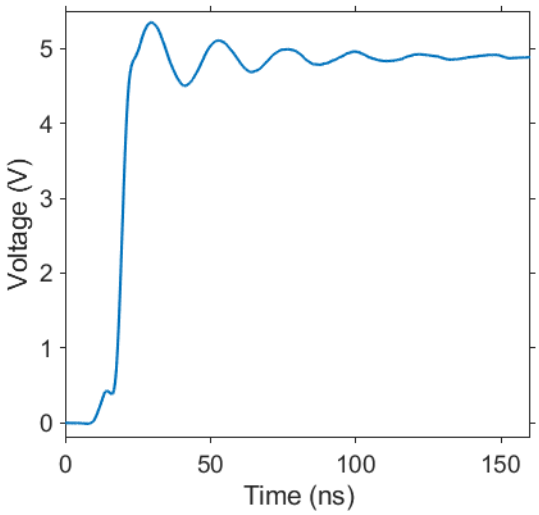

Supplementary Fig. 10| Custom pulse generator employed for the electronic textile. a, Photograph of the pulse generator plugged into the oscilloscope. b, Produced step function captured by the oscilloscope, exhibiting a rise time of approximately 5 ns.

. a

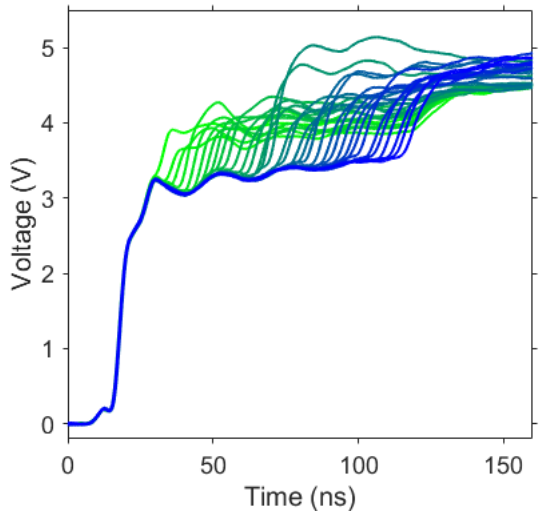

b

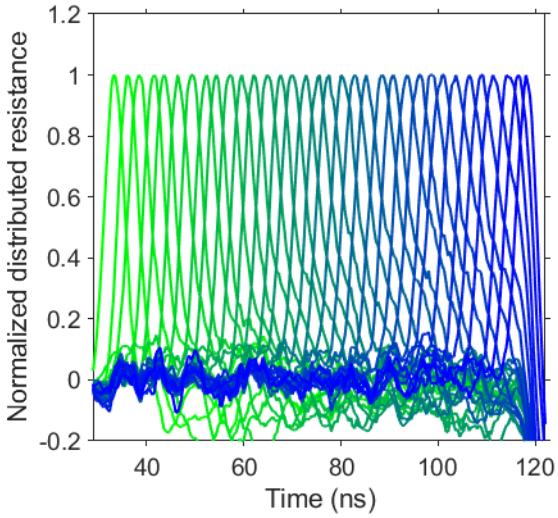

. c

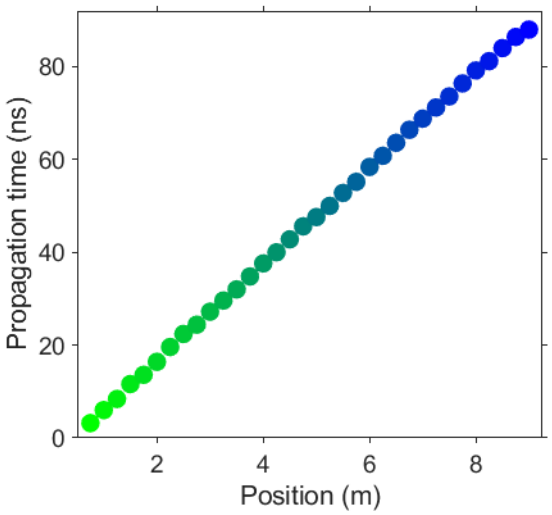

Supplementary Fig. 11| Pressure points are successively applied in 25 cm steps along the length of the soft transmission line, which is integrated in the electronic textile, to approximate the spatial resolution. The color gradient from green to blue indicates the distance of the pressure points from the interrogated end. a, Produced waveforms for the pressure points of similar force magnitudes at gradually increased positions. b, Normalized distributed resistance calculated from the waveforms. c, The propagation time of the signal from the interrogated line end to the discontinuity is extracted and shown as a function of pressure position on the line.

. a b

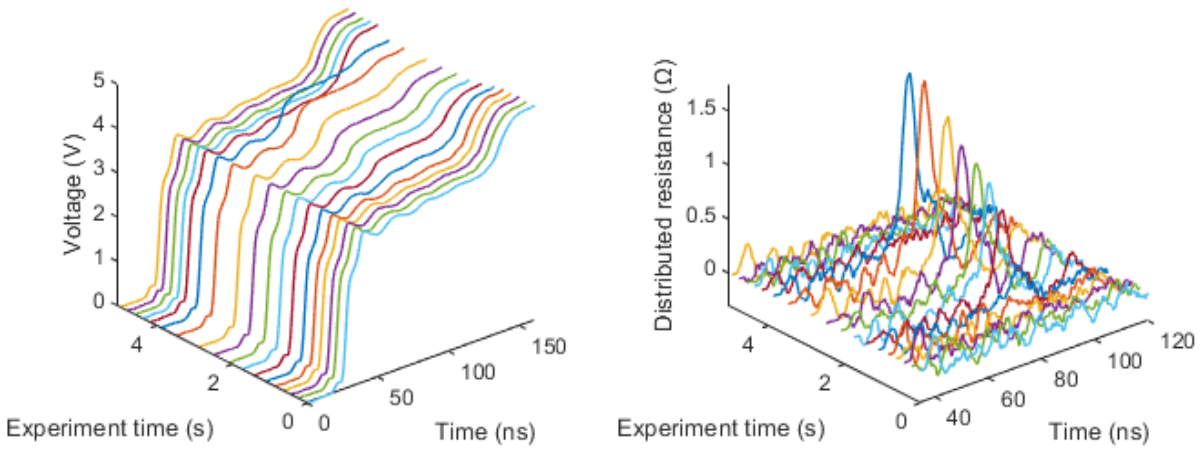

Supplementary Fig. 12| Pressing on electronic textile. Time-domain reflectometry waveforms (a) and calculated distributed resistance (b) for a single point on the transmission line being increasingly compressed by a finger. The height and the time of the resistance peak indicate the pressure magnitude and location, respectively.

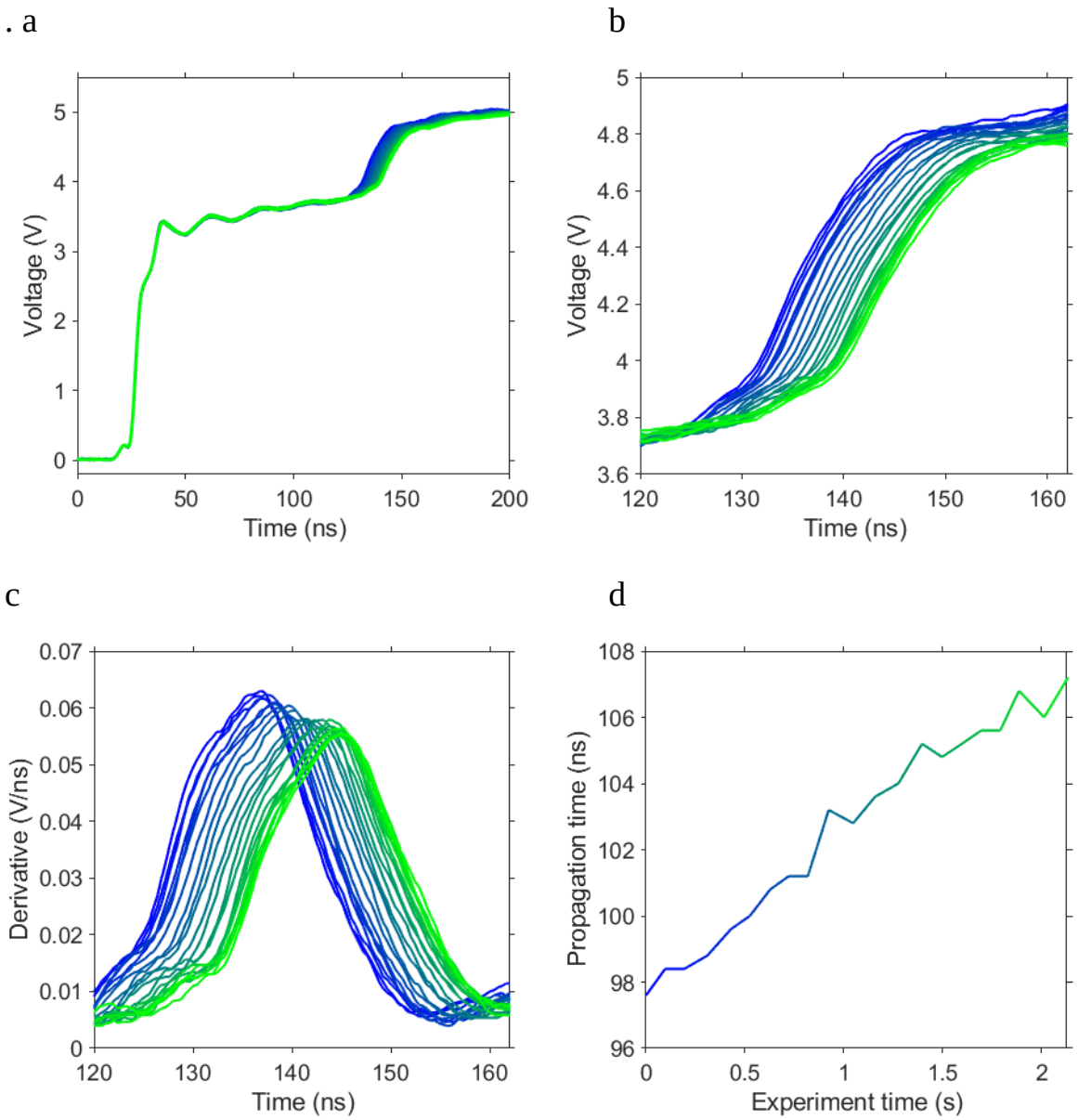

Supplementary Fig. 13| Stretching of electronic textile. Time-domain reflectometry waveforms of transmission line that is increasingly stretched (a and b) and derivate thereof (c). The peak of the derivate is used to identify the propagation time of the signal (d), which is used to calculate line elongation, as shown in Fig. 5d. The color gradient from blue to green is used to indicate the increasing stretch and relates all plots to one another.